Acta Mech 227, 2343–2360 (2016)
DOI 10.1007/s00707-016-1641-2

ORIGINAL PAPER

Keqiang Hu · Zengtao Chen

Strip yield zone of a penny-shaped crack in a magnetoelectroelastic material under axisymmetric loadings

Received: 30 December 2015 / Revised: 31 March 2016 / Published online: 28 April 2016

Abstract The strip yield zone ahead of a penny-shaped crack in a magnetoelectroelastic material, subjected to electric, magnetic and axisymmetric mechanical loadings, is evaluated analytically. Hankel transform is employed to reduce the mixed boundary value problem of the penny-shaped crack to dual integral equations, which are solved exactly under the assumption of electrically and magnetically permeable crack face conditions and the plastic strip yield zone crack model. An analytic solution to the mixed boundary problem has been obtained to predict the relationship between the length of the strip yield zone and the applied loadings. The distribution of mechanical, electric and magnetic fields in and outside of the strip yield zone in the cracked magnetoelectroelastic material has been derived analytically, and the crack opening displacement has been investigated. The effects of the mechanical, electric and magnetic loadings on the size of the yield zone are discussed in detail.

1 Introduction

Composite materials consisting of piezoelectric and piezomagnetic phases exhibit a magnetoelectric effect that is unavailable in single-phase piezoelectric or piezomagnetic materials. Owing to the unique magnetoelectroelastic coupling effect, these kinds of materials can be used in intelligent structures as sensors and actuators. Studies on the properties of piezoelectric/piezomagnetic composites have drawn considerable attention in recent years. Some defects (such as dislocations and cracks) could be induced during the manufacturing processes or during service by the mechanical, electric or magnetic loading, which can adversely influence the performance of the structures. Therefore, it is necessary to advance our understanding of the characteristics of a magnetoelectroelastic material with defects [1].

In recent decades, there is a growing interest among researchers in solving fracture mechanics problems in magnetoelectroelastic media. Gao et al. [2] presented an exact treatment on the problem of an elliptical hole or a crack in a magnetoelectroelastic solid subjected to the far-field loadings by using the Stroh formulation. A family of closed-form thermomagnetoelectroelastic Green's functions for problems of defects in a magnetoelectroelastic solid has been derived by Qin [3] by the use of Stroh's formalism and conforming mapping, and the results can be used to establish boundary element formulation and to analyze relevant fracture problems. Hu and Li [4] analyzed the singular stress, electric and magnetic fields in a piezoelectromagnetic strip containing a Griffith crack under longitudinal shear using the theory of linear piezoelectromagneticity. Li [5] made a transient analysis of a cracked magnetoelectroelastic medium under antiplane mechanical and in-plane electric and magnetic impacts by using the Fourier and Laplace transforms. The dynamic response of a penny-shaped crack in a magnetoelectroelastic layer was studied by Feng et al. [6], and the effects of magnetoelectromechanical loadings, crack surface conditions and crack configuration on crack propagation

K. Hu (✉) · Z. Chen
Department of Mechanical Engineering, University of Alberta, Edmonton, AB T6G 2G8, Canada
E-mail: keqianghu@gmail.com; keqianghu@163.com

and growth have been examined. The boundary element method has been developed by Rojas-Díaz et al. [7] to study crack problems in linear magnetoelectroelastic materials under static loading conditions. Wang and Mai [8] discussed the different electromagnetic boundary conditions on the crack faces in magnetoelectroelastic materials with coupled piezoelectric, piezomagnetic and magnetoelectric effects. Zhong and Li [9] provided a fracture analysis of a magnetoelectroelastic solid with a penny-shaped crack by considering the effects of the opening crack interior. A partially conducting mode I crack in piezoelectromagnetic materials was analyzed by Zhou and Chen [10] by using the Schmidt method. The problem of a planar magnetoelectroelastic layered half-plane subjected to generalized line forces and edge dislocations was analyzed by Ma and Lee [11]. Li and Lee [12] established real fundamental solutions for in-plane magnetoelectroelastic governing equations and studied collinear unequal cracks in magnetoelectroelastic materials. Li et al. [13] obtained analytical solutions for an elliptical cylinder inclusion inside an infinite magnetoelectroelastic medium under combined mechanical–electrical–magnetic loadings via the Stroh formalism, and crack problems of the mode I, mode II and mode III have been investigated when the inclusion becomes a crack. An embedded mixed-mode crack in a functionally graded magnetoelectroelastic infinite medium has been studied by Rekik et al. [14] using the Fourier transform and singular integral equation technique. Wan et al. [15] investigated a mode III crack crossing the magnetoelectroelastic biomaterial interface under concentrated magnetoelectromechanical loads, the Riemann-Hilbert problem was formulated and solved based on complex variable method, and analytical solutions were obtained for the entire plane. Hu and Chen [16] analyzed an opening crack in a magnetoelectroelastic strip under in-plane impacts and found that crack curving may occur under some loading conditions. A pre-kinking analysis of a moving crack in a magnetoelectroelastic material under in-plane loading has been provided by Hu and Chen [17]. Liu et al. [18] investigated a penny-shaped magnetically dielectric crack in a magnetoelectroelastic cylinder, and it shows that the impermeable and permeable crack problems are special cases of their solutions.

The above-mentioned fracture mechanics studies are based on linear theory and predict the singular field around the crack tip, which is physically unrealistic. The crack propagation problem considering the plastic behavior may be investigated by applying the Dugdale model [19]. Fan [20] proposed the moving Dugdale model for the mode I, II and III cracks and verified that dynamic crack opening, sliding and tearing displacements are significant for describing the fracture process of materials with nonlinear behavior. Hoh et al. [21] carried out an analytical investigation on the plastic zone size and crack tip opening displacement of a Dugdale crack interacting with a circular inclusion. Fan et al. [22] investigated the interaction among a Zener-Stroh crack, a nearby inhomogeneity/inclusion and an extra edge dislocation with the distributed dislocation method, and the plastic zone correction at the crack tips is determined.

Various nonlinear models have been suggested to study the crack problems in piezoelectric material. Gao et al. [23] generalized the essential idea of Dugdale [19] and proposed a strip yield saturation model of electrical yielding by assuming that the electrical polarization is saturated in a line segment in front of the crack tips. Narita and Shindo [24] investigated the mode I crack growth rate for the yield strip model of a narrow piezoelectric strip. Zhang et al. [25] proposed a strip dielectric breakdown model and predicted the effect of electric fields on the fracture behavior. Zhao and Fan [26] further proposed the strip electric–magnetic breakdown (SEMB) model for an electrically and magnetically impermeable crack in a magnetoelectroelastic medium to study the effect of the nonlinear character of electric field and magnetic field on the fracture of magnetoelectroelastic materials, and the sizes of the electric breakdown zone and the magnetic breakdown zone have been obtained. Recently, Hu and Chen [27] studied the Dugdale plastic zone of a penny-shaped crack in a piezoelectric material under axisymmetric loading using Hankel transform and the technique of dual integral equations.

It is noted that conventional brittle ceramics can become ductile permitting large plastic deformations at low temperature if a polycrystalline ceramic was fabricated with a crystal size of a few nanometers, and the ductility seems to originate from the dislocation slip processes and diffusional flow of atoms along the intercrystalline interfaces [28,29]. Ferroelectric/ferromagnetic polymers have a ductile mechanical behavior and good piezoelectric/ piezomagnetic properties which make these materials ideal candidates for ceramic particle-reinforced ferroelectric/ferromagnetic composites, where significant ductility is retained [30,31].

To the best knowledge of the authors, the problem of a strip yield zone around a penny-shaped crack in a magnetoelectroelastic material under axisymmetric magnetoelectromechanical loadings has not been reported in the literature. This paper extends the method of Hu and Chen [27], and the mode I strip yield crack problem in magnetoelectroelastic materials is solved in this paper. The crack surfaces are assumed to be electrically and magnetically permeable, and the strip yield zone ahead of the fringe of the penny-shaped crack is considered. Hankel transforms are applied, and the mixed boundary value problem of the crack is reduced to a pair of

dual integral equations, which are solved exactly. The mechanical, electric and magnetic fields near the penny-shaped crack are non-singular, the relation between the yield zone size and the applied loadings is derived, and the crack opening displacement (COD) has been obtained in closed form. The coupling effect of mechanical, electric and magnetic fields on the strip yield zone size and crack opening displacement is investigated.

2 Basic equations for magnetoelectroelastic materials

Consider a transversely isotropic magnetoelectroelastic material with the poling direction along the z-axis and the isotropic plane as the xy-plane. For an axisymmetric problem, the constitutive equations within the framework of the theory of a linear magnetoelectroelastic medium are:

$$\begin{Bmatrix} \sigma_{rr} \\ \sigma_{\theta\theta} \\ \sigma_{zz} \\ D_z \\ B_z \end{Bmatrix} = \begin{bmatrix} C_{11} & C_{12} & C_{13} & e_{31} & h_{31} \\ C_{12} & C_{11} & C_{13} & e_{31} & h_{31} \\ C_{13} & C_{13} & C_{33} & e_{33} & h_{33} \\ e_{31} & e_{31} & e_{33} & -\varepsilon_{33} & -d_{33} \\ h_{31} & h_{31} & h_{33} & -d_{33} & -\mu_{33} \end{bmatrix} \begin{Bmatrix} \frac{\partial u_r}{\partial r} \\ \frac{u_r}{r} \\ \frac{\partial u_z}{\partial z} \\ \frac{\partial \phi}{\partial z} \\ \frac{\partial \varphi}{\partial z} \end{Bmatrix}, \tag{1.1}$$

$$\begin{Bmatrix} \sigma_{rz} \\ D_r \\ B_r \end{Bmatrix} = \begin{bmatrix} C_{44} & e_{15} & h_{15} \\ e_{15} & -\varepsilon_{11} & -d_{11} \\ h_{15} & -d_{11} & -\mu_{11} \end{bmatrix} \begin{Bmatrix} \frac{\partial u_z}{\partial r} + \frac{\partial u_r}{\partial z} \\ \frac{\partial \phi}{\partial r} \\ \frac{\partial \varphi}{\partial r} \end{Bmatrix} \tag{1.2}$$

where the field quantities are functions of r and z, independent of angle θ; u_r and u_z are the radial and axial components of the elastic displacements, respectively; E_j and H_j $(j = r, z)$ are components of electric field and magnetic field, respectively. $\sigma_{rr}, \sigma_{\theta\theta}, \sigma_{zz}, \sigma_{rz}$ are components of stress tensors; D_r and D_z the components of electric displacement vectors; B_r and B_z the components of magnetic induction; $C_{11}, C_{12}, C_{13}, C_{33}, C_{44}$ the elastic moduli; e_{15}, e_{31}, e_{33} the piezoelectric constants; h_{15}, h_{31}, h_{33} the piezomagnetic constants; d_{11}, d_{33} the magnetoelectric constants; $\varepsilon_{11}, \varepsilon_{33}$ the dielectric permittivities; and μ_{11}, μ_{33} the magnetic permeabilities.

The electric field and magnetic field components may be written in terms of the electric potential ϕ and magnetic potential φ, respectively, as:

$$E_r = -\frac{\partial \phi}{\partial r}, \quad E_z = -\frac{\partial \phi}{\partial z}, \tag{2.1}$$

$$H_r = -\frac{\partial \varphi}{\partial r}, \quad H_z = -\frac{\partial \varphi}{\partial z}. \tag{2.2}$$

In the absence of body forces and free charges, the equilibrium equations are:

$$\begin{aligned} \frac{\partial \sigma_{rr}}{\partial r} + \frac{\partial \sigma_{rz}}{\partial z} + \frac{\sigma_{rr} - \sigma_{\theta\theta}}{r} &= 0, \\ \frac{\partial \sigma_{rz}}{\partial r} + \frac{\partial \sigma_{zz}}{\partial z} + \frac{\sigma_{rz}}{r} &= 0, \\ \frac{\partial D_r}{\partial r} + \frac{\partial D_z}{\partial z} + \frac{D_r}{r} &= 0, \\ \frac{\partial B_r}{\partial r} + \frac{\partial B_z}{\partial z} + \frac{B_r}{r} &= 0. \end{aligned} \tag{3}$$

Substitution of Eq. (1) into the above equations leads to the governing equations for the elastic displacements u_r and u_z, electric potential ϕ and magnetic potential φ as follows:

$$
\begin{aligned}
&C_{11}\left(\frac{\partial^2 u_r}{\partial r^2}+\frac{1}{r}\frac{\partial u_r}{\partial r}-\frac{u_r}{r^2}\right)+C_{44}\frac{\partial^2 u_r}{\partial z^2}+(C_{13}+C_{44})\frac{\partial^2 u_z}{\partial r\partial z}+(e_{15}+e_{31})\frac{\partial^2 \phi}{\partial r\partial z}+(h_{15}+h_{31})\frac{\partial^2 \varphi}{\partial r\partial z}=0,\\
&C_{44}\left(\frac{\partial^2 u_z}{\partial r^2}+\frac{1}{r}\frac{\partial u_z}{\partial r}\right)+(C_{13}+C_{44})\left(\frac{\partial^2 u_r}{\partial r\partial z}+\frac{1}{r}\frac{\partial u_r}{\partial z}\right)+C_{33}\frac{\partial^2 u_z}{\partial z^2}+e_{15}\left(\frac{\partial^2 \phi}{\partial r^2}+\frac{1}{r}\frac{\partial \phi}{\partial r}\right)+e_{33}\frac{\partial^2 \phi}{\partial z^2}\\
&\quad+h_{15}\left(\frac{\partial^2 \varphi}{\partial r^2}+\frac{1}{r}\frac{\partial \varphi}{\partial r}\right)+h_{33}\frac{\partial^2 \varphi}{\partial z^2}=0,\\
&(e_{15}+e_{31})\left(\frac{\partial^2 u_r}{\partial r\partial z}+\frac{1}{r}\frac{\partial u_r}{\partial z}\right)+e_{15}\left(\frac{\partial^2 u_z}{\partial r^2}+\frac{1}{r}\frac{\partial u_z}{\partial r}\right)+e_{33}\frac{\partial^2 u_z}{\partial z^2}-\varepsilon_{11}\left(\frac{\partial^2 \phi}{\partial r^2}+\frac{1}{r}\frac{\partial \phi}{\partial r}\right)-\varepsilon_{33}\frac{\partial^2 \phi}{\partial z^2}\\
&\quad-d_{11}\left(\frac{\partial^2 \varphi}{\partial r^2}+\frac{1}{r}\frac{\partial \varphi}{\partial r}\right)-d_{33}\frac{\partial^2 \varphi}{\partial z^2}=0,\\
&(h_{15}+h_{31})\left(\frac{\partial^2 u_r}{\partial r\partial z}+\frac{1}{r}\frac{\partial u_r}{\partial z}\right)+h_{15}\left(\frac{\partial^2 u_z}{\partial r^2}+\frac{1}{r}\frac{\partial u_z}{\partial r}\right)+h_{33}\frac{\partial^2 u_z}{\partial z^2}-d_{11}\left(\frac{\partial^2 \phi}{\partial r^2}+\frac{1}{r}\frac{\partial \phi}{\partial r}\right)-d_{33}\frac{\partial^2 \phi}{\partial z^2}\\
&\quad-\mu_{11}\left(\frac{\partial^2 \varphi}{\partial r^2}+\frac{1}{r}\frac{\partial \varphi}{\partial r}\right)-\mu_{33}\frac{\partial^2 \varphi}{\partial z^2}=0.
\end{aligned}
\tag{4}
$$

3 Problem statement and method of solution

A three-dimensional extension of Dugdale's plastic zone model (Dugdale [19]) in magnetoelectroelastic material is considered in this study. For a penny-shaped crack of radius c under remote mechanical, electric and magnetic loadings applied in the z-direction, a coplanar plastic strip yield ring is formed in front of the crack, as shown in Fig. 1. The crack surfaces are assumed to be electrically and magnetically permeable, and the electric and magnetic fields are not high enough to lead to electric or magnetic breakdown. In order to eliminate the singularity of the mechanical, electric and magnetic fields near the crack tips, we consider a small-scale yield zone ahead of the crack in the magnetoelectroelastic material. It is noted that this kind of plastic zone is an idealized version of the cohesive zone model. Dugdale's hypothesis approximates the size of the plastic yield zone by considering the enlarged crack of radius a with yielding condition satisfied in the plastic yield ring. Cylindrical coordinates r, θ and z are used, the poling direction is along the z-axis, and the penny-shaped

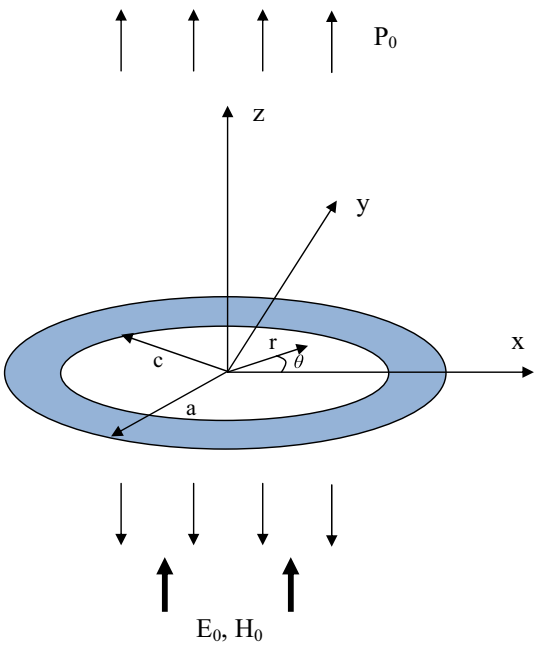

Fig. 1 Dugdale-type strip yield penny-shaped crack in magnetoelectroelastic material

crack occupies the region $r \le c, z = 0$. An axisymmetric normal stress P_0, electric field E_0, and magnetic field H_0 are applied at infinity, as shown in Fig. 1, and it is assumed that there is no external loading applied in the lateral surface at infinity.

Due to the symmetry of the problem, it is sufficient to consider the upper-half space of the cracked magnetoelectroelastic material. The corresponding boundary conditions of the mixed boundary value problem are:

$$\sigma_{zz}(r,0) = \begin{cases} 0 & (0 \le r < c) \\ \sigma_Y & (c \le r < a) \end{cases}, \tag{5.1}$$

$$u_z(r,0) = 0 \quad (a \le r \le \infty), \tag{5.2}$$

$$\sigma_{rz}(r,0) = 0 \quad (r \ge 0), \tag{6}$$

$$\phi(r,0) = 0 \quad (r \ge 0), \tag{7}$$

$$\varphi(r,0) = 0 \quad (r \ge 0). \tag{8}$$

It is noted that the electromagnetic conditions on $z = 0$ are referred to the undeformed crack plane, not to the deformed configuration. Small deformation has been assumed, the crack opening displacement (COD) is small enough to allow such approximation to be reasonable, and the conditions have been adopted widely to treat crack problems [16,24,27,32,33].

Hankel transforms are applied to Eq. (4), and the general expressions for the elastic displacements, electric potential and magnetic potential may be obtained as:

$$u_r(r,z) = \sum_{j=1}^{4} a_j \int_0^\infty A_j(\xi) \exp(-\gamma_j \xi z) J_1(\xi r) d\xi + a_0 r, \tag{9.1}$$

$$u_z(r,z) = \sum_{j=1}^{4} \frac{1}{\gamma_j} \int_0^\infty A_j(\xi) \exp(-\gamma_j \xi z) J_0(\xi r) d\xi + b_0 z, \tag{9.2}$$

$$\phi(r,z) = -\sum_{j=1}^{4} \frac{b_j}{\gamma_j} \int_0^\infty A_j(\xi) \exp(-\gamma_j \xi z) J_0(\xi r) d\xi - c_0 z, \tag{10}$$

$$\varphi(r,z) = -\sum_{j=1}^{4} \frac{d_j}{\gamma_j} \int_0^\infty A_j(\xi) \exp(-\gamma_j \xi z) J_0(\xi r) d\xi - d_0 z \tag{11}$$

where $J_0()$ and $J_1()$ is the zero- and first-order Bessel function of the first kind, respectively. a_0, b_0, c_0, d_0 are constants determined from the far-field loading conditions, and $a_j, b_j, d_j \quad (j = 1,2,3,4)$ are known coefficients defined as:

$$\begin{Bmatrix} a_0 \\ b_0 \end{Bmatrix} = \begin{bmatrix} 2C_{13} & C_{33} \\ C_{11}+C_{12} & C_{13} \end{bmatrix}^{-1} \begin{Bmatrix} P_0 + e_{33}E_0 + h_{33}H_0 \\ e_{31}E_0 + h_{31}H_0 \end{Bmatrix},$$

$$c_0 = E_0,$$

$$d_0 = H_0, \tag{12}$$

$$\begin{Bmatrix} a_j \\ b_j \\ d_j \end{Bmatrix} = \begin{bmatrix} C_{11} - C_{44}\gamma_j^2 & e_{31}+e_{15} & h_{31}+h_{15} \\ (C_{13}+C_{44})\gamma_j^2 & e_{33}\gamma_j^2 - e_{15} & h_{33}\gamma_j^2 - h_{15} \\ (e_{31}+e_{15})\gamma_j^2 & \varepsilon_{11} - \varepsilon_{33}\gamma_j^2 & d_{11} - d_{33}\gamma_j^2 \end{bmatrix}^{-1} \begin{Bmatrix} C_{13}+C_{44} \\ C_{33}\gamma_j^2 - C_{44} \\ e_{33}\gamma_j^2 - e_{15} \end{Bmatrix}. \tag{13}$$

$A_j(\xi), (j = 1,2,3,4)$ are unknowns, and $\gamma_j \ (j = 1,2,3,4)$ are the roots of the following characteristic equation:

$$\begin{vmatrix} C_{11} - C_{44}\gamma^2 & (C_{13}+C_{44})\gamma & (e_{31}+e_{15})\gamma & (h_{31}+h_{15})\gamma \\ (C_{13}+C_{44})\gamma & C_{33}\gamma^2 - C_{44} & e_{33}\gamma^2 - e_{15} & h_{33}\gamma^2 - h_{15} \\ (e_{31}+e_{15})\gamma & e_{33}\gamma^2 - e_{15} & \varepsilon_{11} - \varepsilon_{33}\gamma^2 & d_{11} - d_{33}\gamma^2 \\ (h_{31}+h_{15})\gamma & h_{33}\gamma^2 - h_{15} & d_{11} - d_{33}\gamma^2 & \mu_{11} - \mu_{33}\gamma^2 \end{vmatrix} = 0 \tag{14}$$

where $|\mathbf{M}|$ denotes the determinant of the matrix $\mathbf{M}$.

Note that the eighth-order characteristic Eq. (14) has eight roots which occur in pairs with the same magnitude but opposite signs, and for complex roots, they always appear in conjugate pairs. In the expressions (11), the roots γ_j $(j = 1, 2, 3, 4)$ are chosen as $\mathrm{Re}(\gamma_j) > 0$ by requiring a positive internal energy for the system to be in a steady state, as stated by Hu and Chen [16,17,34], and Re denotes the real part of a complex number. The set of eigenvalues obtained from Eq. (14) is connected to those of the Stroh–Lekhnitskii formalism [35,36] by $p_j = i \cdot \gamma_j$, where p_j are their eigenvalues. A similar connection was established by Chiang and Weng [37] for a penny-shaped dielectric crack in a piezoelectric solid.

The expressions for the stresses, electric displacement and magnetic induction in the cracked magneto-electroelastic body can be obtained as follows:

$$\sigma_{rz} = -\sum_{j=1}^{4} \frac{f_j}{\gamma_j} \int_0^\infty \xi A_j(\xi) \exp(-\gamma_j \xi z) J_1(\xi r) d\xi, \tag{15.1}$$

$$\sigma_{zz} = \sum_{j=1}^{4} g_j \int_0^\infty \xi A_j(\xi) \exp(-\gamma_j \xi z) J_0(\xi r) d\xi + P_0, \tag{15.2}$$

$$D_z = \sum_{j=1}^{4} s_j \int_0^\infty \xi A_j(\xi) \exp(-\gamma_j \xi z) J_0(\xi r) d\xi + D_0, \tag{15.3}$$

$$B_z = \sum_{j=1}^{4} t_j \int_0^\infty \xi A_j(\xi) \exp(-\gamma_j \xi z) J_0(\xi r) d\xi + B_0, \tag{15.4}$$

$$\begin{aligned} D_0 &= \frac{e_{33} P_0 + (e_{33}^2 + C_{33}\varepsilon_{33}) E_0 + (e_{33} h_{33} + C_{33} d_{33}) H_0}{C_{33}}, \\ B_0 &= \frac{h_{33} P_0 + (e_{33} h_{33} + C_{33} d_{33}) E_0 + (h_{33}^2 + C_{33}\mu_{33}) H_0}{C_{33}} \end{aligned} \tag{16}$$

where the coefficients $f_j, g_j, s_j, t_j (j = 1, 2, 3, 4)$ are defined as:

$$\begin{aligned} f_j &= C_{44}(a_j \gamma_j^2 + 1) - e_{15} b_j - h_{15} d_j, \\ g_j &= C_{13} a_j + e_{33} b_j + h_{33} d_j - C_{33}, \\ s_j &= e_{31} a_j - \varepsilon_{33} b_j - d_{33} d_j - e_{33}, \\ t_j &= h_{31} a_j - d_{33} b_j - \mu_{33} d_j - h_{33}. \end{aligned} \quad (j = 1, 2, 3, 4) \tag{17}$$

It can be observed from Eqs. (15, 16) that the far-field loading conditions are satisfied automatically, and the normal stress P_0 may be expressed as

$$P_0 = \sigma_0 - e_{33} E_0 - h_{33} H_0 \tag{18}$$

where σ_0 is the uniform normal stress at zero electric and magnetic loads.

By substituting Eqs. (9–16) into the boundary conditions (6–8), the following relations hold:

$$\sum_{j=1}^{4} f_j A_j(\xi)/\gamma_j = 0, \tag{19.1}$$

$$\sum_{j=1}^{4} b_j A_j(\xi)/\gamma_j = 0, \tag{19.2}$$

$$\sum_{j=1}^{4} d_j A_j(\xi)/\gamma_j = 0. \tag{19.3}$$

It is noted that Eqs. (19.2) and (19.3) are derived from the boundary conditions in Eqs. (7) and (8), respectively, and Eqs. (7) and (8) assume that the crack surfaces are electrically and magnetically permeable [16].

By solving the above linear equations, $A_j(\xi)$, $(j = 1-4)$ can be expressed as functions of the only independent unknown function $E(\xi)$ as:

$$A_j(\xi) = \gamma_j \Delta_j E(\xi), \quad (j = 1-4) \tag{20}$$

where the constants $\Delta_j \quad (j = 1-4)$ are given as

$$\Delta_1 = b_2(d_3 f_4 - d_4 f_3) + b_3(d_4 f_2 - d_2 f_4) + b_4(d_2 f_3 - d_3 f_2), \tag{21.1}$$
$$\Delta_2 = b_1(d_4 f_3 - d_3 f_4) + b_3(d_1 f_4 - d_4 f_1) + b_4(d_3 f_1 - d_1 f_3), \tag{21.2}$$
$$\Delta_3 = b_1(d_2 f_4 - d_4 f_2) + b_2(d_4 f_1 - d_1 f_4) + b_4(d_1 f_2 - d_2 f_1), \tag{21.3}$$
$$\Delta_4 = b_1(d_3 f_2 - d_2 f_3) + b_2(d_1 f_3 - d_3 f_1) + b_3(d_2 f_1 - d_1 f_2). \tag{21.4}$$

Satisfaction of the mixed boundary conditions (7) on the crack face leads to the dual integral equations as follows:

$$\int_0^\infty \xi \sum_{j=1}^{4} g_j A_j(\xi) J_0(\xi r) d\xi = \begin{cases} -P_0 & (0 \le r < c) \\ -P_0 + \sigma_Y & (c \le r < a) \end{cases}, \tag{22.1}$$

$$\int_0^\infty \sum_{j=1}^{4} \frac{A_j(\xi)}{\gamma_j} J_0(\xi r) d\xi = 0 \quad (r \ge a). \tag{22.2}$$

Substitution of the expression of Eq. (20) leads to the dual integral equations for the unknown function $E(\xi)$:

$$\int_0^\infty \xi E(\xi) J_0(\xi r) d\xi = F(r), \quad (0 \le r < a), \tag{23.1}$$

$$\int_0^\infty E(\xi) J_0(\xi r) d\xi = 0 \quad (r \ge a) \tag{23.2}$$

where the function $F(r)$ is defined as:

$$F(r) = \begin{cases} -\frac{P_0}{G_0} & (0 \le r < c) \\ \frac{\sigma_Y - P_0}{G_0} & (c \le r < a) \end{cases} \tag{24.1}$$

with

$$G_0 = \sum_{j=1}^{4} g_j \gamma_j \Delta_j. \tag{24.2}$$

The set of dual integral Eq. (23) may be obtained by introducing a new function defined by

$$E(\xi) = \int_0^a Y(t) \sin(\xi t) \mathrm{d}t. \tag{25}$$

It is observed that Eq. (23.2) is satisfied automatically, the satisfaction of Eq. (23.1) leads to an Abel integral equation for $Y(t)$, and the solution can be expressed as

$$Y(t) = \frac{2}{\pi} \int_0^t \frac{r F(r)}{\sqrt{t^2 - r^2}} \mathrm{d}r. \tag{26}$$

The detailed derivation of this solution is provided in the Appendix of Hu and Chen [27].

The stress intensity factor K_I for the penny-shaped crack can be defined as

$$K_I = \lim_{x \to a^+} \sqrt{2(r-a)} \sigma_{zz}(r, 0) = -G_0 \frac{Y(a)}{\sqrt{a}}. \tag{27}$$

Based on the assumption of the strip yield crack model, when the penny-shape-cracked body is under remote axisymmetric loadings, a ring-shaped yield zone is accumulated in the region $c < r < a$, where a closure

stress equal to σ_Y is applied to remove the singularity at the crack fronts $r = a$. Hence, the following condition must be satisfied:

$$Y(a) = 0 \tag{28}$$

for the vanishing stress intensity factor K_I. It should be noted that this condition also leads to the non-singular electric displacement and magnetic induction in the cracked magnetoelectroelastic material, i.e.,

$$K_D = \lim_{x \to a^+} \sqrt{2(r-a)} D_z(r,0) = -s_0 \frac{Y(a)}{\sqrt{a}} = 0, \tag{29.1}$$

$$K_B = \lim_{x \to a^+} \sqrt{2(r-a)} B_z(r,0) = -t_0 \frac{Y(a)}{\sqrt{a}} = 0 \tag{29.2}$$

where the constants s_0 and t_0 are given as

$$\begin{aligned} s_0 &= \sum_{j=1}^{4} s_j \gamma_j \Delta_j, \\ t_0 &= \sum_{j=1}^{4} t_j \gamma_j \Delta_j. \end{aligned} \tag{30}$$

Due to the linear relationship of the constitutive equations of the magnetoelectroelastic materials, the electric and magnetic fields in the cracked body are non-singular.

4 Yield zone size

The relationship involving the applied normal stress P_0, the normal yield stress σ_Y, the original crack length c, and the effective crack length a can be obtained from substituting Eqs. (24, 26) into Eq. (28).

Using Eqs. (24) and (26), it follows

$$F(r) = \begin{cases} -\frac{P_0}{G_0} = f_0 & (0 \le r < c) \\ \frac{\sigma_Y}{G_0} = \sigma_S & (c \le r < a) \end{cases}, \tag{31}$$

$$\begin{aligned} Y(t) &= \frac{2}{\pi} \int_0^t \frac{r\,[f_0 + \sigma_S \mathbf{H}(x-c)]}{\sqrt{t^2 - r^2}} dr \\ &= \begin{cases} \frac{2}{\pi} f_0 t & (0 \le t < c) \\ \frac{2}{\pi} f_0 t + \frac{2}{\pi} \sigma_S \sqrt{t^2 - c^2} & (c \le t < a) \end{cases} \end{aligned} \tag{32}$$

where $\mathbf{H}(x)$ is the Heaviside step function.

From the above equations and Eq. (28), the relationship between the size of the yield zone and the applied load can be determined as

$$\frac{c}{a} = \sqrt{1 - \left(\frac{P_0}{\sigma_Y}\right)^2}. \tag{33}$$

This result is in agreement with the solution for a Dugdale-type penny-shaped crack in isotropic and transversely isotropic materials [38,39].

The substitution of Eq. (18) into Eq. (33) leads to the result

$$\frac{c}{a} = \sqrt{1 - \left(\frac{\sigma_0}{\sigma_Y}\right)^2 (1 - L_E - L_H)^2} \tag{34}$$

where L_E and L_H are the parameters for the electric and magnetic loadings, respectively, defined as:

$$\begin{aligned} L_E &= \frac{e_{33} E_0}{\sigma_0}, \\ L_H &= \frac{h_{33} H_0}{\sigma_0}. \end{aligned} \tag{35}$$

5 Non-singular field distribution near crack tip

The stresses, electric displacements, magnetic inductions, electric fields and magnetic fields in the cracked magnetoelectroelastic material are non-singular due to the assumption of the strip yield zone model and an electrically and magnetically permeable crack. By substituting Eqs. (20), (25), (32) into Eqs. (15) (see details in the Appendix) the non-singular stress, electric displacement, magnetic induction, electric field and magnetic field on the crack face plane can be obtained as:

$$\sigma_{zz}(r,0) = P_0 + \frac{2}{\pi}\left\{\frac{\sigma_Y}{2}\left[\tan^{-1}\left(\frac{2a^2-c^2-r^2}{2\sqrt{a^2-c^2}\sqrt{r^2-a^2}}\right)+\frac{\pi}{2}\right]-P_0\tan^{-1}\left(\frac{a}{\sqrt{r^2-a^2}}\right)\right\}, \quad (r \geq a) \tag{36}$$

$$\sigma_{zz}(r,0) = \sigma_Y \mathbf{H}(r-c), \quad (0 \leq r < a) \tag{37}$$

$$D_z(r,0) = D_0 + \frac{2s_0}{\pi G_0}\left\{\frac{\sigma_Y}{2}\left[\tan^{-1}\left(\frac{2a^2-c^2-r^2}{2\sqrt{a^2-c^2}\sqrt{r^2-a^2}}\right)+\frac{\pi}{2}\right]-P_0\tan^{-1}\left(\frac{a}{\sqrt{r^2-a^2}}\right)\right\}, \quad (r \geq a) \tag{38}$$

$$D_z(r,0) = D_0 + \frac{s_0}{G_0}\left[\sigma_Y \mathbf{H}(r-c) - P_0\right], \quad (0 \leq r < a) \tag{39}$$

$$B_z(r,0) = B_0 + \frac{2t_0}{\pi G_0}\left\{\frac{\sigma_Y}{2}\left[\tan^{-1}\left(\frac{2a^2-c^2-r^2}{2\sqrt{a^2-c^2}\sqrt{r^2-a^2}}\right)+\frac{\pi}{2}\right]-P_0\tan^{-1}\left(\frac{a}{\sqrt{r^2-a^2}}\right)\right\}, \quad (r \geq a) \tag{40}$$

$$B_z(r,0) = B_0 + \frac{t_0}{G_0}\left[\sigma_Y \mathbf{H}(r-c) - P_0\right], \quad (0 \leq r < a) \tag{41}$$

$$E_z(r,0) = E_0 - \frac{2b_*}{\pi G_0}\left\{\frac{\sigma_Y}{2}\left[\tan^{-1}\left(\frac{2a^2-c^2-r^2}{2\sqrt{a^2-c^2}\sqrt{r^2-a^2}}\right)+\frac{\pi}{2}\right]-P_0\tan^{-1}\left(\frac{a}{\sqrt{r^2-a^2}}\right)\right\}, \quad (r \geq a) \tag{42}$$

$$E_z(r,0) = E_0 - \frac{b_*}{G_0}\left[\sigma_Y \mathbf{H}(r-c) - P_0\right], \quad (0 \leq r < a) \tag{43}$$

$$H_z(r,0) = H_0 - \frac{2d_*}{\pi G_0}\left\{\frac{\sigma_Y}{2}\left[\tan^{-1}\left(\frac{2a^2-c^2-r^2}{2\sqrt{a^2-c^2}\sqrt{r^2-a^2}}\right)+\frac{\pi}{2}\right]-P_0\tan^{-1}\left(\frac{a}{\sqrt{r^2-a^2}}\right)\right\}, \quad (r \geq a) \tag{44}$$

$$H_z(r,0) = H_0 - \frac{d_*}{G_0}\left[\sigma_Y \mathbf{H}(r-c) - P_0\right], \quad (0 \leq r < a) \tag{45}$$

where

$$b_* = \sum_{j=1}^{4} b_j \gamma_j \Delta_j,$$
$$d_* = \sum_{j=1}^{4} d_j \gamma_j \Delta_j. \tag{46}$$

It can be observed that the electric and magnetic fields are disturbed by the presence of the crack and the strip yield zone. If there is no crack in the magnetoelectroelastic material, the stress, electric and magnetic fields are all constant fields. It is noted that because the prescribed traction in the yield zone has a discontinuity at $r = c$, there is a singular point at $r = c$. From Eqs. (36–41), we can see that the stress, electric displacement and magnetic induction in the yield zone are uniform, the electric displacement and magnetic induction are of constant values on the crack faces, while the crack faces are stress-free. Equations (42–45) show the normal components of the electric field and magnetic field, which are discontinuous at the physical crack edge ($r = c$), as shown in terms of the step function $\mathbf{H}(r - c)$, while at the mathematical crack edge ($r = a$) the normal

components of the stress, electric displacement, magnetic induction, electric and magnetic fields are continuous, as shown in Eqs. (36–45).

The expression of the normal stress near the crack tip can be obtained as:

$$\sigma_{zz}(r,z) = P_0 + \int_0^a Y'(t) \sum_{j=1}^{4} \int_0^\infty \delta_j \exp(-\gamma_j \xi z) \cos(\xi t) J_0(\xi r) d\xi \mathrm{d}t. \tag{47}$$

By using the integral identity

$$\int_0^\infty \exp(-\beta x) \cos(\alpha x) J_0(xt) \mathrm{d}x = \sqrt{\frac{\sqrt{(\beta^2+t^2-\alpha^2)^2+4\alpha^2\beta^2}+\beta^2+t^2-\alpha^2}{2\left[(\beta^2+t^2-\alpha^2)^2+4\alpha^2\beta^2\right]}} \tag{48}$$

we can obtain the explicit expression of the stress around the crack as

$$\sigma_{zz}(r,z) = P_0 + \sum_{j=1}^{4} \delta_j \int_0^a Y'(t) \Omega_j(\gamma_j, t, r, z) \mathrm{d}t, \quad (r \geq a), \tag{49}$$

$$\sigma_{zz}(r,z) = P_0 + \sum_{j=1}^{4} \delta_j \int_0^r Y'(t) \Omega_j(\gamma_j, t, r, z) \mathrm{d}t, \quad (0 \leq r < a) \tag{50}$$

where

$$\begin{aligned} \Omega_j(\gamma_j, t, r, z) &= \int_0^\infty \exp(-\gamma_j z\xi) \cos(t\xi) J_0(r\xi) \mathrm{d}\xi \\ &= \sqrt{\frac{\sqrt{(\gamma_j^2 z^2 + r^2 - t^2)^2 + 4t^2\gamma_j^2 z^2} + \gamma_j^2 z^2 + r^2 - t^2}{2\left[(\gamma_j^2 z^2 + r^2 - t^2)^2 + 4t^2\gamma_j^2 z^2\right]}}, \end{aligned} \tag{51}$$

$$\delta_j = g_j \gamma_j \Delta_j. \tag{52}$$

The detailed expression of the normal stress in different regions can be further given in the following form:

$$\sigma_{zz}(r,z) = P_0 + \frac{2}{\pi} \sum_{j=1}^{4} \delta_j \left\{ f_0 \int_0^a \Omega_j(\gamma_j, t, r, z) \mathrm{d}t + \sigma_S \int_c^a \frac{t}{\sqrt{t^2 - c^2}} \Omega_j(\gamma_j, t, r, z) \mathrm{d}t \right\}, \quad (r \geq a) \tag{53.1}$$

$$\sigma_{zz}(r,z) = P_0 + \frac{2}{\pi} \sum_{j=1}^{4} \delta_j \left\{ f_0 \int_0^r \Omega_j(\gamma_j, t, r, z) \mathrm{d}t + \sigma_S \int_c^r \frac{t}{\sqrt{t^2 - c^2}} \Omega_j(\gamma_j, t, r, z) \mathrm{d}t \right\}, \quad (c \leq r < a) \tag{53.2}$$

$$\sigma_{zz}(r,z) = P_0 + \frac{2}{\pi} \sum_{j=1}^{4} \delta_j \left\{ f_0 \int_0^r \Omega_j(\gamma_j, t, r, z) dt \right\}, \quad (0 \leq r < c). \tag{53.3}$$

Similar expressions for the distribution of the electric and magnetic fields can be obtained and are omitted here. It is noted that the general solution of the mechanical, electric and magnetic fields in the cracked magnetoelectroelastic material is easily calculated by numerical integration.

COD is an important parameter to represent the fracture mechanics property of cracked materials under applied loadings, and the concept of COD offers an opportunity to examine size effects in fracture in a logical and controlled manner [40]. The COD for the current crack problem can be obtained as

$$\begin{aligned} \mathrm{COD}(r) &= 2u_z(r,0) \\ &= \frac{4d_0}{\pi G_0} \left\{ \sigma_Y \int_c^a \frac{\sqrt{\eta^2 - c^2}}{\sqrt{\eta^2 - r^2}} d\eta - P_0 \sqrt{a^2 - r^2} \right\} \quad (0 \leq r < c), \end{aligned} \tag{54.1}$$

$$\mathrm{COD}(r) = \frac{4d_0}{\pi G_0}\left\{\sigma_Y \int_r^a \frac{\sqrt{\eta^2 - c^2}}{\sqrt{\eta^2 - r^2}} d\eta - P_0\sqrt{a^2 - r^2}\right\} \quad (c \le r \le a) \tag{54.2}$$

where $d_0 = \sum_{j=1}^{4} \Delta_j$ and G_0 is defined in Eq. (24.2).

The COD at the original crack fringe ($r = c$), i.e., the crack tip opening displacement (CTOD), can be obtained as

$$\mathrm{CTOD} = \mathrm{COD}(c) = \frac{4d_0}{\pi G_0} c\left[\sqrt{\sigma_Y^2 - P_0^2} - \sigma_Y\right]. \tag{55}$$

It is noted that the CTOD is related to the far-field loadings, the material parameters and the yield stress of the material. The constants d_0 and G_0 are related to the characteristic roots of the material and are dependent on the material properties. When $P_0 = 0$, it is clear that the CTOD vanishes, and when $P_0 \to \sigma_Y$, the CTOD goes to a limit value of $-\frac{4d_0}{\pi G_0} c\sigma_Y$, which is positive (if $\sigma_Y > 0$) and related to the loading and material properties.

6 Numerical results

The magnetoelectroelastic material is taken to be a transversely isotropic material exhibiting full coupling between mechanical, electric and magnetic fields, with the polarized direction perpendicular to the crack plane. In the following numerical computation, the yield stress in the yield zone is assumed to be $\sigma_Y = 100$ MPa without loss of generality, and the material constants of $BaTiO_3$-$CoFe_2O_4$ composite are [41–43]:

$$\begin{aligned}
&C_{11} = 17.8 \times 10^{10}\,(\mathrm{N/m^2}),\ C_{13} = 8.72 \times 10^{10}\,(\mathrm{N/m^2}),\ C_{33} = 17.28 \times 10^{10}\,(\mathrm{N/m^2}),\\
&C_{44} = 4.32 \times 10^{10}\,(\mathrm{N/m^2}),\ e_{15} = 10.44\,(\mathrm{C/m^2}),\ e_{31} = -3.96\,(\mathrm{C/m^2}),\\
&e_{33} = 16.74\,(\mathrm{C/m^2}),\ h_{15} = 55\,(\mathrm{N/Am}),\ h_{31} = 58.03\,(\mathrm{N/Am}),\\
&h_{33} = 69.97\,(\mathrm{N/Am}),\ \varepsilon_{11} = 100.9 \times 10^{-10}\,(\mathrm{C^2/Nm^2}),\ \varepsilon_{33} = 113.5 \times 10^{-10}\,(\mathrm{C^2/Nm^2}),\\
&\mu_{11} = 6.35 \times 10^{-5}\,(\mathrm{Ns^2/C^2}),\ \mu_{33} = 2.47 \times 10^{-5}\,(\mathrm{Ns^2/C^2}),\\
&d_{11} = 5.367 \times 10^{-12}\,(\mathrm{Ns/VC}),\ d_{33} = 2737.5 \times 10^{-12}\,(\mathrm{Ns/VC}).
\end{aligned} \tag{56}$$

The roots of the characteristic Eq. (14) and the quantities d_0 and G_0 can be obtained as

$$\begin{aligned}
&\gamma_1 = 1.1480,\ \gamma_2 = 1.6077,\ \gamma_3 = 0.9318 + 0.0351i,\ \gamma_4 = 0.9318 - 0.0351i,\\
&d_0 = -4.9781 \times 10^{28} i,\ G_0 = 3.3127 \times 10^{39} i.
\end{aligned} \tag{57}$$

The normalized COD's of the penny-shaped crack in three dimensions are displayed in Fig. 2. Without loss of generality, the applied normal stress is taken to be $\sigma_0 = 0.2\sigma_Y$, the magnitudes of the electric and magnetic loading parameters are chosen as $L_E = -0.3$ and $L_H = -0.2$ for the numerical results shown in Fig. 2a,

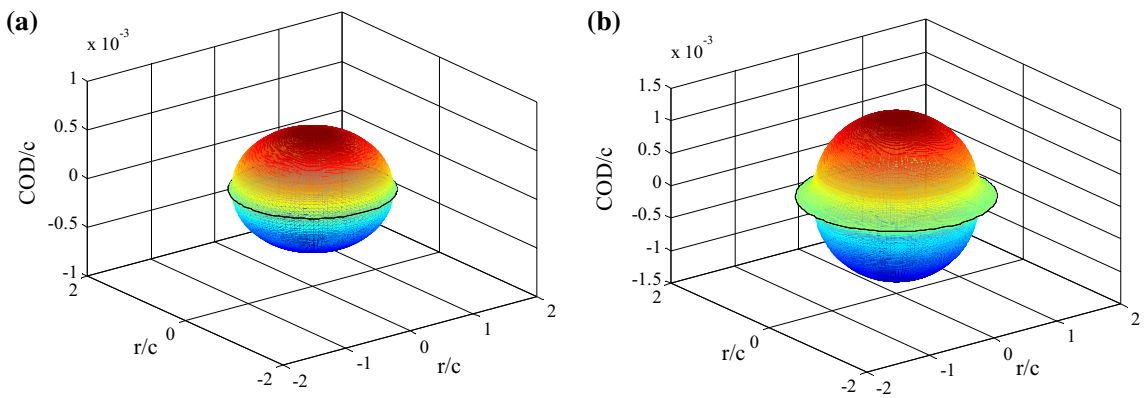

Fig. 2 **a** Normalized COD when $\sigma_0 = 0.2\sigma_Y$, $L_E = -0.3$ and $L_H = -0.2$. **b** Normalized COD when $\sigma_0 = 0.4\sigma_Y$, $L_E = -0.3$ and $L_H = -0.2$

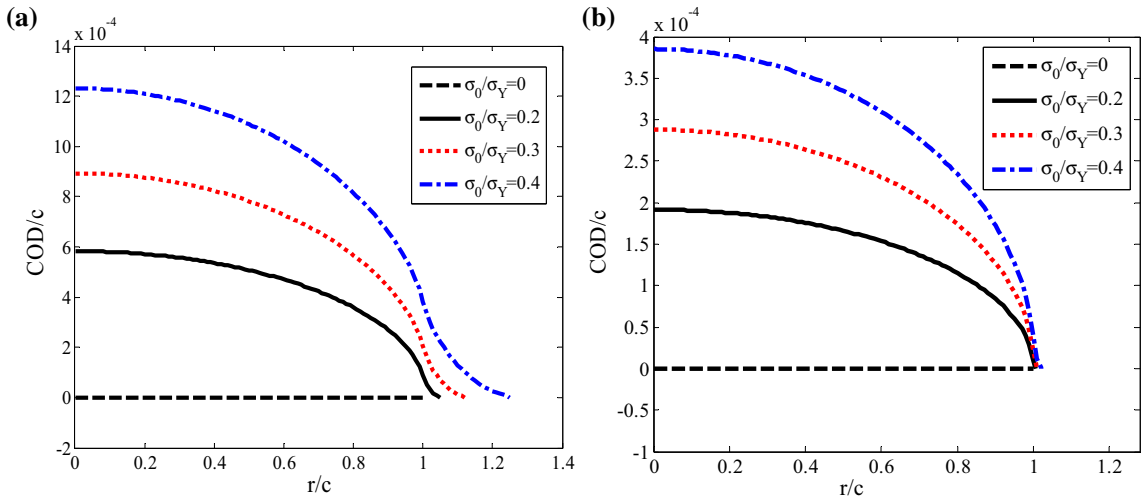

Fig. 3 **a** Normalized COD versus r under different normal stresses when $L_E = -0.3$, $L_H = -0.2$. **b** Normalized COD versus r under different normal stresses when $L_E = +0.3$, $L_H = +0.2$

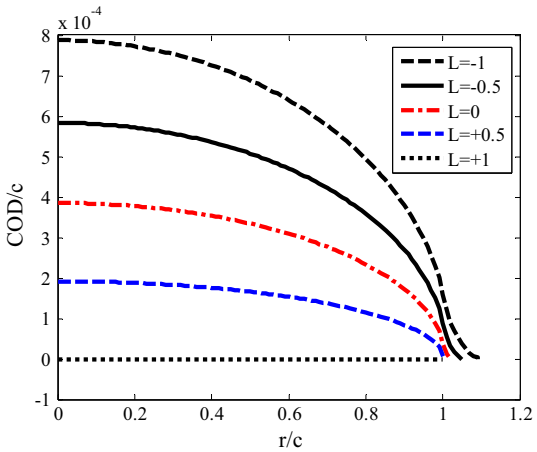

Fig. 4 Normalized COD versus r at different electromagnetic loadings $L = L_E + L_H$ when $\sigma_0 = 0.2\sigma_Y$

while the results shown in Fig. 2b correspond to the loading parameters $L_E = +0.3$ and $L_H = +0.2$. It is noted that "negative" means that the direction of the electric and magnetic loading is opposite to the poling direction. It can be observed from Fig. 2 that the COD of the penny-shaped crack is axisymmetric due to the fact that the loadings and material properties are axisymmetric. The magnitude of the COD due to the negative electric and magnetic loading parameters is larger than that due to the positive electric and magnetic loading parameters.

The normalized CODs under different normal stresses σ_0 are displayed in Fig. 3 for the penny-shaped crack with a strip yield zone in a magnetoelectroelastic material. The CODs under negative electric and magnetic loadings are displayed in Fig. 3a, and the CODs under positive electric and magnetic loadings are shown in Fig. 3b for comparison. The magnitude of the CODs increases as the normal stress σ_0 increases, and the size of the plastic yield zone increases accordingly. The CODs of the penny-shaped crack under negative electric and magnetic loadings are larger than those under positive electric and magnetic loadings.

Figure 4 shows the normalized CODs at different electric and magnetic loadings $L = L_E + L_H$ when $\sigma_0 = 0.2\sigma_Y$. It is observed that the magnitude of CODs and the size of the corresponding plastic yield zone decrease as the loading parameter increases from negative to positive values. It is noted that the COD is zero when $L = L_E + L_H = 1$, as the corresponding normal stress $P_0 = 0$, and there is no plastic yield zone in this case. This result can also be observed from Eqs. (33) and (34). The normalized crack tip opening displacements (CTODs) under different normal stresses P_0 are displayed in Fig. 5 for the penny-shaped crack

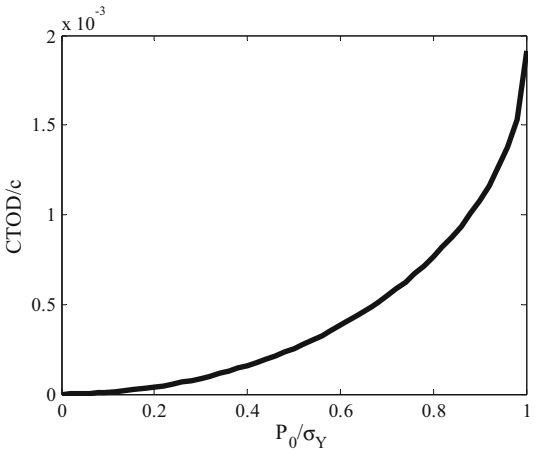

Fig. 5 Normalized CTOD versus normal stress

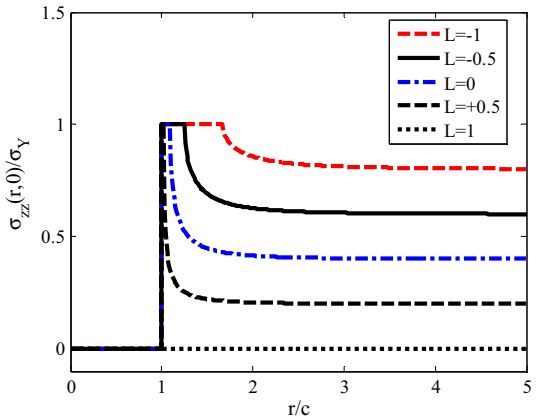

Fig. 6 Stresses on the crack plane at different electro-magnetic loadings when $\sigma_0 = 0.4\sigma_Y$

in a magnetoelectroelastic material. The magnitude of the CTODs increases as the far-field normal stress P_0 increases.

It can be observed from Figs. 2, 3, 4, and 5 that the crack opening displacement (COD) is small enough which guarantees that the result is reasonable based on the approximation of boundary values on the crack faces which are referred to the undeformed crack plane rather than the deformed configuration.

Figure 6 shows the stresses on the crack face plane at different electromagnetic loadings ($L = L_E + L_H$) when $\sigma_0 = 0.4\sigma_Y$. It shows that the crack surfaces are stress-free, the stresses in the plastic zone are equal to the yielding stress σ_Y, and the stress decreases outside of the yield zone and converges to a steady value when it is far enough from the crack. The magnitude of the steady value increases as the electric and magnetic loading parameter $L = L_E + L_H$ decreases from positive to negative values. When $L = 1$, there is no far-field normal stress applied, and the stress level on the crack face plane is zero.

Figure 7 displays the normalized electric field on the crack face plane under different electric loadings L_E when $\sigma_0 = 0.4\sigma_Y$ and $L_H = 0$. It shows that the electric field on the crack faces is constant and is another constant in the yield zone. The electric field on the crack face plane changes gradually outside the yield zone and goes to a steady value which is the same as the far-field electric loading. The normalized magnetic field on the crack face plane under different magnetic loadings L_H when $\sigma_0 = 0.4\sigma_Y$ and $L_E = 0$ is shown in Fig. 8. Similar to the distribution of the electric field on the crack faces and in the yield zone, the magnetic field is constant on the crack faces and in the yield zone. It is noted that this particular distribution of the electric and magnetic fields on the crack faces and in the yield zone is due to the assumption of the Dugdale-type strip yield crack and the electrically and magnetically permeable crack model. It can be observed from Figs. 7 and 8 that the electric and magnetic fields are discontinuous at the edge of the penny-shaped crack, which is analogous to the distribution of stress on the crack faces and ahead of the crack. This phenomenon is due to the constitutive equations of the material and the particular boundary conditions of the crack problem.

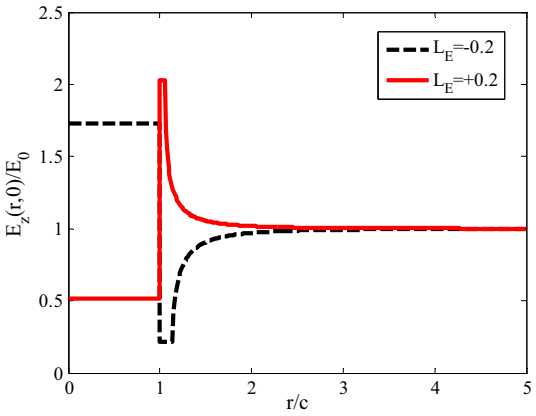

Fig. 7 Electric field on the crack plane when $\sigma_0 = 0.4\sigma_Y$ and $L_H = 0$

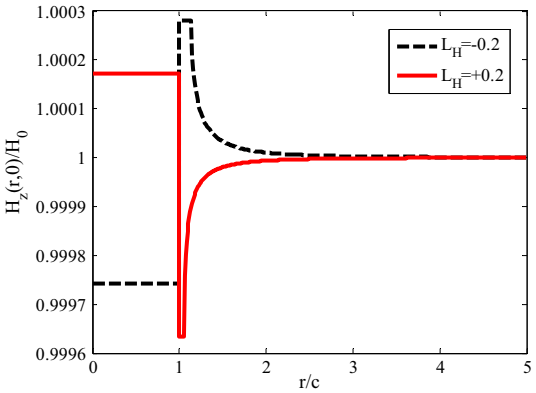

Fig. 8 Magnetic field on the crack plane when $\sigma_0 = 0.4\sigma_Y$ and $L_E = 0$

7 Conclusions

A Dugdale-type strip yield penny-shaped crack in a magnetoelectroelastic material under in-plane mechanical, electric and magnetic loadings is studied under electrically and magnetically permeable crack surface conditions. The non-singular fields near the penny-shaped crack are obtained in an explicit form, and the crack opening displacement and the crack tip opening displacement have been obtained. The yield zone size is affected by the mechanical, electric and magnetic loadings and the yield stress of the magnetoelectroelastic material, while the COD is also related to the material properties. Numerical results indicate that negative electric and magnetic loadings may lead to larger COD, and positive electric and magnetic loadings may lead to smaller COD. The electric and magnetic fields on the crack faces and in the yield zone are constant values due to the assumption of the Dugdale-type strip yield crack and the electrically and magnetically permeable crack model.

Acknowledgments The authors gratefully acknowledge the insightful and constructive comments of the reviewers which have greatly improved the quality of this paper.

Appendix

The function $E(\xi)$ can be obtained by integration from Eq. (25) as

$$E(\xi) = \int_0^a Y(t)\sin(\xi t)\mathrm{d}t = -\frac{Y(a)}{\xi}\cos(\xi a) + \int_0^a Y'(t)\frac{\cos(\xi t)}{\xi}\mathrm{d}t \tag{58}$$

where the fact that $Y(0) = 0$ has been applied considering Eq. (26).

The normal stress on the crack face plane can be obtained as

$$\begin{aligned}\sigma_{zz}(r,0) &= \sum_{j=1}^{4} g_j \int_0^\infty \xi A_j(\xi) J_0(\xi r)\mathrm{d}\xi + P_0 \\ &= P_0 + G_0 \int_0^\infty \xi E(\xi) J_0(\xi r)\mathrm{d}\xi \\ &= P_0 + G_0 \int_0^\infty \left[-Y(a)\cos(\xi a) + \int_0^a Y'(t)\cos(\xi t)dt\right] J_0(\xi r)\mathrm{d}\xi. \end{aligned} \tag{59}$$

Using the identity

$$\int_0^\infty J_0(\xi r)\cos(\xi a)\mathrm{d}\xi = \begin{cases} 0, & (0 < r < a) \\ \frac{1}{\sqrt{r^2-a^2}}, & (r > a) \end{cases} \tag{60}$$

and considering Eqs. (28) and (32), we can get the following result:

$$\begin{aligned}\sigma_{zz}(r,0) &= P_0 + G_0\left[-\frac{Y(a)}{\sqrt{r^2-a^2}} + \int_0^a \frac{Y'(t)}{\sqrt{r^2-t^2}}\mathrm{d}t\right] \\ &= P_0 + G_0 \int_0^a \frac{Y'(t)}{\sqrt{r^2-t^2}}\mathrm{d}t \\ &= P_0 + G_0\left[\frac{2f_0}{\pi}\int_0^a \frac{1}{\sqrt{r^2-t^2}}\mathrm{d}t + \frac{2\sigma_S}{\pi}\int_c^a \frac{1}{\sqrt{1-(c/t)^2}\sqrt{r^2-t^2}}\mathrm{d}t\right] \quad (r \geq a). \end{aligned} \tag{61}$$

By using the following identities:

$$\begin{aligned}\int_0^a \frac{1}{\sqrt{r^2-t^2}}dt &= \tan^{-1}\left[\frac{a}{\sqrt{r^2-a^2}}\right] \\ \int_c^a \frac{1}{\sqrt{1-(c/t)^2}\sqrt{r^2-t^2}}\mathrm{d}t &= \frac{1}{2}\left\{\tan^{-1}\left[\frac{2a^2-c^2-r^2}{2\sqrt{a^2-c^2}\sqrt{r^2-a^2}}\right] + \frac{\pi}{2}\right\} \end{aligned} \tag{62}$$

and the relations in Eqs. (31), we can get

$$\sigma_{zz}(r,0) = P_0 + \frac{2}{\pi}\left\{\frac{\sigma_Y}{2}\left[\tan^{-1}\left(\frac{2a^2-c^2-r^2}{2\sqrt{a^2-c^2}\sqrt{r^2-a^2}}\right) + \frac{\pi}{2}\right] - P_0\tan^{-1}\left(\frac{a}{\sqrt{r^2-a^2}}\right)\right\}, \quad (r \geq a) \tag{63}$$

which is the same as shown in Eq. (36).

When $c \leq r < a$, considering the identity

$$\int_0^\infty J_0(\xi r)\cos(\xi t)\mathrm{d}\xi = \begin{cases} 0, & (r < t) \\ \frac{1}{\sqrt{r^2-t^2}}, & (r > t) \end{cases}, \tag{64}$$

$$\begin{aligned}\int_0^r \frac{1}{\sqrt{r^2-t^2}}dt &= \tan^{-1}\left[\frac{t}{\sqrt{r^2-t^2}}\right]_0^r = \frac{\pi}{2}, \\ \int_c^r \frac{1}{\sqrt{1-(c/t)^2}\sqrt{r^2-t^2}}\mathrm{d}t &= \frac{1}{2}\tan^{-1}\left[\frac{2t^2-c^2-r^2}{2\sqrt{t^2-c^2}\sqrt{r^2-t^2}}\right]_c^r = \frac{\pi}{2}, \end{aligned} \tag{65}$$

we can get the normal component of stress inside the yield zone as:

$$\begin{aligned}\sigma_{zz}(r,0) &= P_0 + G_0 \int_0^r \frac{Y'(t)}{\sqrt{r^2-t^2}}\mathrm{d}t \\ &= P_0 + G_0 \left[\frac{2f_0}{\pi} \int_0^r \frac{1}{\sqrt{r^2-t^2}}\mathrm{d}t + \frac{2\sigma_S}{\pi} \int_c^r \frac{1}{\sqrt{1-(c/t)^2}\sqrt{r^2-t^2}}\mathrm{d}t \right] \qquad (c \le r < a) \\ &= P_0 + G_0 [f_0 + \sigma_S] \\ &= \sigma_Y . \end{aligned} \tag{66}$$

When $0 \le r < c$, the normal component of stress on the crack faces can be obtained as

$$\begin{aligned}\sigma_{zz}(r,0) &= P_0 + G_0 \int_0^r \frac{Y'(t)}{\sqrt{r^2-t^2}}\mathrm{d}t \\ &= P_0 + G_0 \left[\frac{2f_0}{\pi} \int_0^r \frac{1}{\sqrt{r^2-t^2}}\mathrm{d}t \right] \quad (0 \le r \le c) \\ &= P_0 + G_0 f_0 \\ &= 0. \end{aligned} \tag{67}$$

Equations (66) and (67) can be combined to be

$$\sigma_{zz}(r,0) = \sigma_Y \mathbf{H}(r-c), \quad (0 \le r < a) \tag{68}$$

which is the same as Eq. (37).

Similarly, we can get the results for the normal components of electric displacement and magnetic induction on the crack face plane:

$$D_z(r,0) = D_0 + \sum_{j=1}^{4} s_j \int_0^\infty \xi A_j(\xi) J_0(\xi r)\mathrm{d}\xi = D_0 + s_0 \int_0^\infty \xi E(\xi) J_0(\xi r)\mathrm{d}\xi, \tag{69}$$

$$B_z(r,0) = B_0 + \sum_{j=1}^{4} t_j \int_0^\infty \xi A_j(\xi) J_0(\xi r)\mathrm{d}\xi = B_0 + t_0 \int_0^\infty \xi E(\xi) J_0(\xi r)\mathrm{d}\xi. \tag{70}$$

By using the results from Eqs. (59) to (67), we can obtain the results of $D_z(r,0)$ and $B_z(r,0)$ as shown in Eqs. (38–41).

From Eqs. (59) and (68), it is obvious that

$$\int_0^\infty \xi E(\xi) J_0(\xi r) d\xi = \frac{1}{G_0} [\sigma_Y \mathbf{H}(r-c) - P_0], \quad (0 \le r < a). \tag{71}$$

The normal components of the electric and magnetic fields on the crack face plane can be obtained as

$$\begin{aligned} E(r,0) &= -\sum_{j=1}^{4} b_j \int_0^\infty A_j(\xi) J_0(\xi r)\mathrm{d}\xi + E_0 \\ &= E_0 - b_* \int_0^\infty \xi E(\xi) J_0(\xi r)\mathrm{d}\xi \\ &= E_0 - \frac{b_*}{G_0} [\sigma_Y \mathbf{H}(r-c) - P_0], \quad (0 \le r < a) \\ H(r,0) &= -\sum_{j=1}^{4} d_j \int_0^\infty A_j(\xi) J_0(\xi r) d\xi + H_0 \\ &= H_0 - d_* \int_0^\infty \xi E(\xi) J_0(\xi r)\mathrm{d}\xi \end{aligned} \tag{72}$$

$$= H_0 - \frac{d_*}{G_0}\left[\sigma_Y \mathbf{H}(r-c) - P_0\right], \quad (0 \le r < a). \tag{73}$$

Equations (72) and (73) indicate that the normal components of the electric and magnetic fields on the crack face plane are discontinuous at the physical crack edge ($r = c$), and the corresponding values on the crack face ($0 \le r < c$) and inside the yield zone ($c \le r < a$) are different constants; these results are reasonable due to the fact that stress components are linearly dependent on the electric and magnetic fields. It should be noted that the displacement component normal to the surface at the crack tip should be continuous, while the strain and stress components normal to the surface at the crack tip can allow discontinuities.

References

1. Hu, K.Q., Li, G.Q.: Constant moving crack in a magnetoelectroelastic material under anti-plane shear loading. Int. J. Solids Struct. **42**, 2823–2835 (2005)
2. Gao, C.F., Hannes, K., Herbert, B.: Crack problems in magnetoelectroelastic solids. Part I: exact solution of a crack. Int. J. Eng. Sci. **41**, 969–981 (2003)
3. Qin, Q.H.: 2D Green's functions of defective magnetoelectroelastic solids under thermal loading. Eng. Anal. Bound. Elem. **29**, 577–585 (2005)
4. Hu, K.Q., Li, G.Q.: Electro-magneto-elastic analysis of piezoelectromagnetic strip with a finite crack under longitudinal shear. Mech. Mater. **37**, 925–934 (2005)
5. Li, X.F.: Dynamic analysis of a cracked magnetoelectroelastic medium under antiplane mechanical and inplane electric and magnetic impacts. Int. J. Solids Struct. **42**, 3185–3205 (2005)
6. Feng, W.J., Pan, E., Wang, X.: Dynamic fracture analysis of a penny-shaped crack in a magnetoelectroelastic layer. Int. J. Solids Struct. **44**, 7955–7974 (2007)
7. Rojas-Díaz, R., Garcia-Sanchez, F., Saez, A., Zhang, C.: Fracture analysis of magnetoelectroelastic composite materials. Key Eng. Mater. Adv. Fract. Damage Mech. VI **348–349**, 69–72 (2007)
8. Wang, B.-L., Mai, Y.-W.: Applicability of crack-face electromagnetic boundary conditions for fracture of magnetoelectroelastic materials. Int. J. Solids Struct. **44**, 387–398 (2007)
9. Zhong, X.C., Li, X.F.: Fracture analysis of a magnetoelectroelastic solid with a penny-shaped crack by considering the effects of the opening crack interior. Int. J. Eng. Sci. **46**, 374–390 (2008)
10. Zhou, Z.G., Chen, Z.T.: Fracture mechanics analysis of a partially conducting mode I crack in piezoelectromagnetic materials. Eur. J. Mech. A/Solids **27**, 824–846 (2008)
11. Ma, C.-C., Lee, J.-M.: Theoretical analysis of generalized loadings and image forces in a planar magnetoelectroelastic layered half-plane. J. Mech. Phys. Solids **57**, 598–620 (2009)
12. Li, Y.D., Lee, K.Y.: Collinear unequal crack series in magnetoelectroelastic materials: Mode I case solved via new real fundamental solutions. Eng. Fract. Mech. **77**, 2772–2790 (2010)
13. Li, G., Wang, B.-L., Han, J.-C.: Exact solution for elliptical inclusion in magnetoelectroelastic materials. Int. J. Solids Struct. **47**, 419–426 (2010)
14. Rekik, M., El-Borgi, S., Ounaies, Z.: An embedded mixed-mode crack in a functionally graded magnetoelectroelastic infinite medium. Int. J. Solids Struct. **49**, 835–845 (2012)
15. Wan, Y.P., Yue, Y.P., Zhong, Z.: A mode III crack crossing the magnetoelectroelastic biomaterial interface under concentrated magnetoelectromechanical loads. Int. J. Solids Struct. **49**, 3008–3021 (2012)
16. Hu, K.Q., Chen, Z.T.: Pre-curving analysis of an opening crack in a magnetoelectroelastic strip under in-plane impact loadings. J. Appl. Phys. **112**, 124911 (2012)
17. Hu, K.Q., Chen, Z.T.: Pre-kinking of a moving crack in a magnetoelectroelastic material under in-plane loading. Int. J. Solids Struct. **50**, 2667–2677 (2013)
18. Liu, L.L., Feng, W.J., Ma, P.: A penny-shaped magnetically dielectric crack in a magnetoelectroelastic cylinder under magnetoelectromechanical loads. ZAMMZ. Angew. Math. Mech. **96**, 179–190 (2016)
19. Dugdale, D.S.: Yielding of steel sheets containing slits. J. Mech. Phys. Solids **8**, 100–104 (1961)
20. Fan, T.Y.: Moving Dugdale model. ZAMP **38**, 630–641 (1987)
21. Hoh, H.J., Xiao, Z.M., Luo, J.: On the plastic zone size and crack tip opening displacement of a Dugdale crack interacting with a circular inclusion. Acta Mech. **210**, 305–314 (2010)
22. Fan, M., Xiao, Z.M., Luo, J.: On the plastic zone correction of a Zener–Stroh crack interacting with a nearby inhomogeneity and an edge dislocation. Acta Mech. **226**, 4173–4188 (2015)
23. Gao, H., Zhang, T.-Y., Tong, P.: Local and global energy release rates for an electrically yielded crack in a piezoelectric ceramics. J. Mech. Phys. Solids **45**, 491–509 (1997)
24. Narita, F., Shindo, Y.: Mode I crack growth rate for yield strip model of a narrow piezoelectric ceramic body. Theor. Appl. Fract. Mech. **36**, 73–85 (2001)
25. Zhang, T.Y., Zhao, M.H., Gao, C.F.: The strip dielectric breakdown model. Int. J. Fract. **132**, 311–327 (2005)
26. Zhao, M.-H., Fan, C.-Y.: Strip electric-magnetic breakdown model in magnetoelectro-elastic medium. J. Mech. Phys. Solids **56**, 3441–3458 (2008)
27. Hu, K.Q., Chen, Z.T.: Dugdale plastic zone of a penny-shaped crack in a piezoelectric material under axisymmetric loading. Acta Mech. (2015). doi:10.1007/s00707-015-1501-5
28. Karch, J., Birringer, R., Gleiter, H.: Ceramics ductile at low temperature. Nature **330**, 556–558 (1987)
29. Arturo, D.-R., Diego, G.-G., Eugenio, Z.-S., James, Z.S., Rachman, C.: Making ceramics ductile at low temperatures. Scripta Mater. **56**, 89–91 (2007)

30. Capsal, J.-F., Dantras, E., Laffont, L., Lacabanne, C.: Nanotexture influence of BaTiO3 particles on piezoelectric behaviour of PA 11/BaTiO3 nanocomposites. J. Non-Crystall. Solids **356**, 629–34 (2010)
31. Daga, A., Ganesan, N., Shanker, K.: Harmonic response of three-phase magneto-electro-elastic beam under mechanical, electrical and magnetic environment. J. Intell. Mater. Syst. Struct. **20**, 1203–1220 (2009)
32. Li, X.F.: Electroelastic analysis of an anti-plane shear crack in a piezoelectric ceramic strip. Int. J. Solids Struct. **39**, 1097–1117 (2002)
33. Li, S.: On global energy release rate of a permeable crack in piezoelectric ceramic. J. Appl. Mech. **70**, 246–252 (2003)
34. Hu, K.Q., Chen, Z.T., Zhong, Z.: Pre-kinking analysis of a constant moving crack in a magnetoelectroelastic strip under in-plane loading. Eur. J. Mech. A/Solids **43**, 25–43 (2014)
35. Stroh, A.N.: Steady state problems in anisotropic elasticity. J. Math. Phys. **41**, 77–103 (1962)
36. Lekhnitskii, S.G.: Theory of Elasticity of an Anisotropic Elastic Body. Holden-Day, Inc., San Francisco (1963)
37. Chiang, C.-R., Weng, G.J.: Nonlinear behavior and critical state of a penny-shaped dielectric crack in a piezoelectric solid. J. Appl. Mech. **74**, 852–860 (2007)
38. Olesiak, Z., Wnuk, M.: Plastic energy dissipation due to a penny-shaped crack. Int. J. Fract. **4**, 383–396 (1968)
39. Li, X.-Y., Gu, S.-T., He, Q.-C., Chen, W.-Q.: Penny-shaped Dugdale crack in a transversely isotropic medium and under axisymmetric loading. Math. Mech. Solids **18**, 246–263 (2012)
40. Burdekin, F.M., Stone, D.E.W.: The crack opening displacement approach to fracture mechanics in yielding materials. J. Strain Anal. **1**, 145–153 (1966)
41. Huang, J.H., Kuo, W.-S.: The analysis of piezoelectric/piezomagnetic composite materials containing ellipsoidal inclusions. J. Appl. Phys. **81**, 1378–1386 (1997)
42. Song, Z.F., Sih, G.C.: Crack initiation behaviour in magnetoelectroelastic composite under in-plane deformation. Theor. Appl. Fract. Mech. **39**, 189–207 (2003)
43. Tian, W.Y., Rajapakse, R.K.N.D.: Fracture analysis of magnetoelectroelastic solids using path independent integrals. Int. J. Fract. **131**, 311–335 (2005)